1. INFLUENCE OF SOIL STRUCTURE ON THE EVOLUTION OF SMALL-STRAIN SHEAR MODULUS DURING DRYING–WETTING CYCLES

Abstract

Hydroclimatic variability intensifies suction fluctuations in near-surface tropical soils, directly affecting stiffness at small strains and, consequently, serviceability performance of shallow foundations and earth structures. This study investigates the evolution of small-strain shear stiffness of a natural lateritic clayey soil from southern Brazil subjected to controlled drying and wetting paths under unconfined conditions. Thirty-three tests were performed on specimens prepared in three structural states: undisturbed, remoulded at field void ratio, and compacted at standard compaction energy. Hydraulic paths were imposed on the same specimen to ensure consistency in structural history and to capture hysteretic effects. Suction was obtained from the soil-water retention curve following ASTM D5298, and small-strain stiffness was measured after hydraulic equilibration using bender elements. Results demonstrate a systematic increase in small-strain stiffness during drying and a reduction during wetting, evidencing hydraulic hysteresis in the mechanical response. Compacted specimens exhibited consistently higher stiffness and reduced sensitivity at low water contents, followed by a pronounced degradation beyond a threshold moisture range. Remoulded specimens showed marked structural instability under wetting, with progressive disaggregation associated with the loss of natural cementation at high void ratio. The results confirm that structural condition governs both the magnitude of initial stiffness and its path-dependency under hydraulic cycling. The findings provide experimental evidence linking suction-controlled stiffness to microstructural stability in lateritic soils and highlight the necessity of incorporating hydraulic path effects into stiffness-based design frameworks for tropical unsaturated deposits.

Keywords lateritic soil; unsaturated behaviour; small-strain shear Stiffness; bender element testing; drying–wetting cycles; hydraulic hysteresis.

1.1. INTRODUCTION

Climate change has been inducing alterations in the magnitude, intensity, and temporal distribution of precipitation events, thereby increasing the complexity of problems associated with soil-structure interaction. This scenario has motivated a growing body of research aimed at understanding the implications of such variations on the performance and safety of geotechnical structures, with soil type playing a significant role in the observed mechanical response (Booshehrian et al., 2020; Insana et al., 2025; Kandalai et al., 2023; Kilsby et al., 2009; Olaiz et al., 2021; Pham, 2025; Pham and Sutman, 2023; Tetteh et al., 2025). In this context, unsaturated soils assume a central role, as they are commonly encountered in nature, particularly within near-surface soil layers, engineered fills, and regions subjected to seasonal climatic variability. Such soils are also characteristic of arid and semi-arid environments, as well as areas with deep groundwater tables, where matric suction exerts a significant influence on their hydraulic and mechanical behaviour (Pham and Sutman, 2023).

In southern Brazil, the region addressed in the present study, unsaturated soils are predominantly found within near-surface deposits and natural slopes. In recent years, the increasing frequency of extreme precipitation events has resulted in adverse and, in some cases, catastrophic impacts on geotechnical structures founded on these soils, as well as on the stability of natural and engineered slopes. Rainfall infiltration associated with high-intensity events promotes a progressive loss of matric suction within residual soils, leading to a reduction in shear strength and an increased susceptibility to instability (Pham, 2025). These regional manifestations highlight the need to understand how large-scale climatic drivers are translated into soil-scale hydro-mechanical responses.

At the soil scale, the translation of regional climatic processes into mechanical behaviour depends largely on soil properties such as permeability, water retention behaviour, and hydraulic conductivity, which govern infiltration dynamics, matric suction loss, and pore-water pressure fluctuations during wetting–drying (Pham, 2025). Among the mechanical parameters influenced by these processes, the shear resistance mobilised at small strain levels, G_0, plays a key role in controlling the initial stiffness response of unsaturated soils (Gao et al., 2025; Ngoc et al., 2019; Walker et al., 2023).

Accordingly, a substantial body of experimental research has focused on the relationship between suction and small-strain stiffness. A consistent outcome of previous investigations is that the small-strain shear modulus is linked to suction (Dong et al.,

2016; Hoyos et al., 2015; Liu et al., 2020; Ng and Yung, 2008). Nevertheless, hysteresis effects have been observed in small-strain stiffness, indicating that the dependence of G_0 on suction may be nonlinear (e.g., Ng and Yung 2008b; Dong et al. 2016). Experimental studies combining bender element testing and suction-controlled resonant column tests have shown that G_0 of moderately unsaturated soils increases with matric suction following a power-law relationship (Hoyos et al., 2015; Ng and Yung, 2008).

1.2. MATERIAL, SPECIMEN PREPARATION AND TESTING PROGRAMME

1.2.1. Materials

The tested material was collected from an experimental geotechnical engineering field site located in southern Brazil (Masutti et al., 2023). The location of the study area is shown in Figure 1-1, together with the geographical distribution of sands and clays exhibiting lateritic behaviour across the Brazilian territory, as proposed by Villibor and Nogami (2009). According to this mapping, the sampling site is located within a region characterised by clayey soils with lateritic behaviour.

Figure 1-1. Location of the study area and distribution of lateritic soils in Brazil.

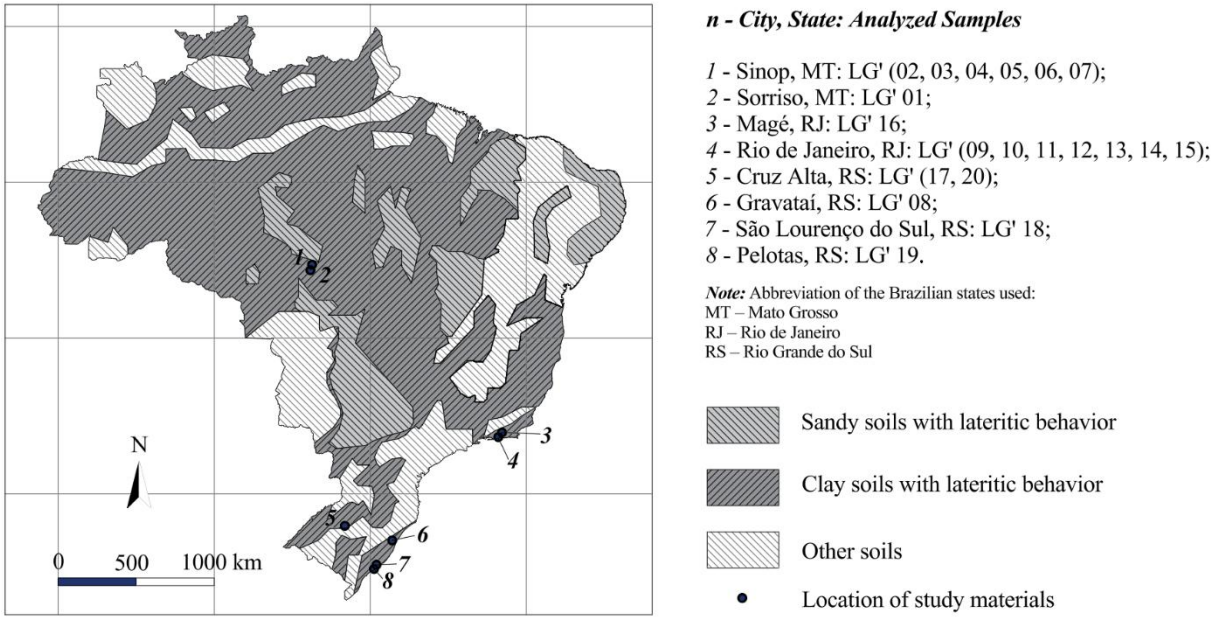

Tropical soils, particularly those with a lateritic structure, exhibit microstructural and mineralogical features that are not adequately represented by conventional soil

classification systems developed for temperate climates, such as the Unified Soil Classification System (ASTM D2487-17, 2020) and the Highway Research Board (ASTM D2487-17, 2020)classification. Owing to these limitations, NOGAMI and VILLIBOR (1981)proposed the MCT (Miniature, Compacted, Tropical) methodology, specifically developed for characterizing and classifying tropical soils.

According to the MCT classification, soils are subdivided into lateritic and non-lateritic materials. As presented in Table 1, which summarises the physical and chemical characterisation of the investigated material, the soil is classified as LG', corresponding to a lateritic clayey soil. This classification is consistent with observations previously reported for tropical soils developed under similar geological and climatic conditions (Pascoal et al., 2023, 2021).

Chemical characterisation indicates that the solid fraction of the soil is predominantly composed of iron and aluminium oxides, associated with the presence of minerals such as gibbsite, which are responsible for the formation of stable aggregates. This microstructural arrangement is reflected in the particle size distribution curves obtained with and without the use of a dispersing agent, highlighting the influence of cementation and aggregation typical of lateritic soils.

Table 1-1. Physical and mineralogical features of the test soil.

Properties	**Value**
Natural dry density (kN/m³)	11.45
Natural moisture content (%)	32.56
Void Index	1.39
Degree of Saturation (%)	64
Liquid limit (%)	46
Plastic Limit (%)	30
Plastic Index (%)	16
Specific gravity (kN/m³)	27,20
XRD analysis	Kaolinite, Gibbsite

Source: Author (2026).

1.2.2. Specimen Preparation and Testing Programme

Drying and wetting cycles were applied to lateritic soil specimens prepared under three distinct structural conditions, namely undisturbed, remoulded and compacted, to investigate the evolution of small-strain shear stiffness. All experiments were conducted under unconfined conditions. Before hydraulic cycling, baseline measurements of the small-strain shear modulus, G_0, were obtained for each specimen condition to establish

the initial stiffness state of the material. The evolution of dry unit weight and water content during the cycles is presented in Figure 1-2.

A total of 33 experimental tests were carried out. Undisturbed specimens were carefully trimmed to cylindrical dimensions of 50 mm in diameter and 100 mm in height. These specimens were tested over a wide range of water contents, varying from 12% to 37%, corresponding to degrees of saturation between 30% and 77%.

Remoulded specimens were statically reconstituted to reproduce the void ratio and water content of the undisturbed specimens, thereby allowing a direct comparison between these two structural conditions. The corresponding preparation parameters are summarised in Table 1-1. Compacted specimens were prepared based on the compaction curve obtained under standard Proctor energy (Figure 1-2), resulting in an optimum water content of 23.34% and a dry unit weight of approximately 14.90 kN/m³. For this preparation condition, the tests encompassed water contents ranging from 9% to 29%.

Figure 1-2. Dry unit weight–water content paths during unconfined hydraulic cycling: (a) IUC, (b) RUC and (c) CUC.

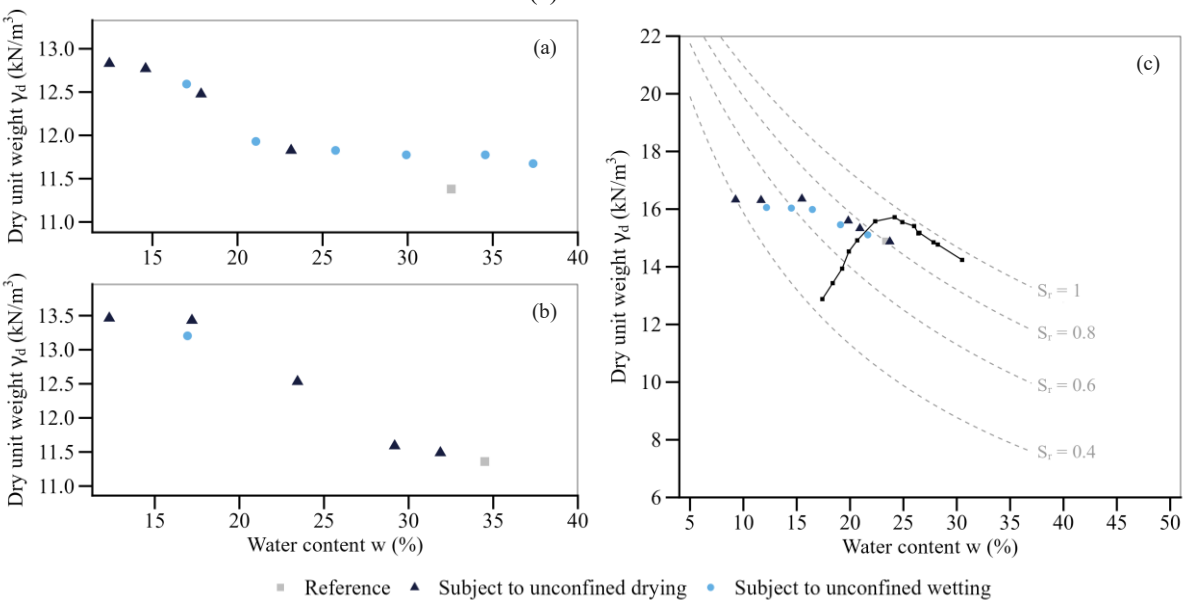

For the unconfined drying and wetting programme, hydraulic cycling was performed by subjecting each specimen to successive stages of drying and wetting, using the same specimen throughout the entire sequence to capture hysteretic effects. The initial states adopted for the unconfined drying and wetting tests are detailed in Table 1-2, where IUC, RUC and CUC denote undisturbed, remoulded and compacted specimens, respectively.

Drying stages were achieved by exposing the specimens to ambient air in a temperature-controlled environment maintained at 20 ± 2 °C. Wetting stages were carried out through the controlled spraying of distilled water onto the specimen surface. Progression along the drying and wetting paths was monitored by continuous measurement of specimen mass. Matric suction was subsequently inferred from the soil water characteristic curve, following the procedures recommended in ASTM D5298 (2010).

After each imposed hydraulic stage, the specimens were isolated to prevent moisture exchange with the environment and stored under sealed conditions for a stabilisation period of approximately 10 days. This procedure was adopted to promote internal moisture redistribution and to ensure a uniform suction state before mechanical assessment. Once stabilisation was achieved, the small-strain shear modulus, G_0, was measured using bender element testing. Changes in specimen volume throughout the drying and wetting sequence were quantified from repeated measurements of height and diameter using a calliper. The degrees of saturation corresponding to each hydraulic state are reported in Table 2. To preserve hydraulic continuity and avoid cumulative disturbance effects, each drying and wetting path was carried out on a single specimen for each preparation condition.

Table 1-2. Initial specimen states and hydraulic paths are considered in the experimental programme.

Sample	Dry unit weight (kN/m³)	Initial void ratio	Saturation Degree- S_r	S_r at each step
IUC	11.38	1.390	0.54	0.64 → 0.48 → 0.41 → 0.35 → 0.30 → 0.40 → 0.45 → 0.54 → 0.62 → 0.72 → 0.76
RUC	11.36	1.394	0.67	0.67 → 0.63 → 0.59 → 0.54 → 0.46 → 0.33 → 0.43
CUC	14.89	0.826	0.77	0.77 → 0.97 → 0.78 → 0.74 → 0.73 → 0.64 → 0.47 → 0.38 → 0.48 → 0.57 → 0.64 → 0.68 → 0.74

1.2.3. Experimental techniques

Shear wave propagation velocities were determined in this study using the bender element technique, which has been widely employed in laboratory investigations aimed at assessing soil stiffness at very small strain levels. In general, this technique has been applied in experimental studies involving different soil types under a range of hydraulic conditions and stress states, allowing the estimation of the initial shear stiffness from

elastic wave propagation (e.g. Viggiani and Atkinson 1995b; Lee and Santamarina 2005; Gu et al. 2013; Camacho-Tauta et al. 2014, 2015; Shahgholian et al. 2025). In the context of the present work, the bender element technique was adopted to quantify the evolution of soil stiffness during drying and wetting cycles carried out under unconfined conditions, thereby enabling the investigation of stiffness variations associated solely with changes in the hydraulic state of the material.

The experimental system consisted essentially of a function generator responsible for producing the electrical excitation signals and a data acquisition system used to record both the input and output signals. To allow adequate visualization and interpretation of the acquired signals, an ultrasonic pre-amplifier was incorporated into the experimental setup before signal acquisition. All measurements were performed using a bender element system (Owntec, version 1) developed for laboratory applications in soils. Figure 1-3a schematically illustrates the testing configuration, including the arrangement of the piezoelectric elements installed at the extremities of cylindrical specimens with a diameter of 50 mm and a height of 100 mm. As the tests were conducted under unconfined conditions, a bench-top configuration was adopted, ensuring that the measurements reflected only the effects associated with variations in soil moisture content.

Figure 1-3. (a) Bender element test configuration for unconfined specimens. (b) Input and output signals showing peak-to-peak determination of shear wave travel time.

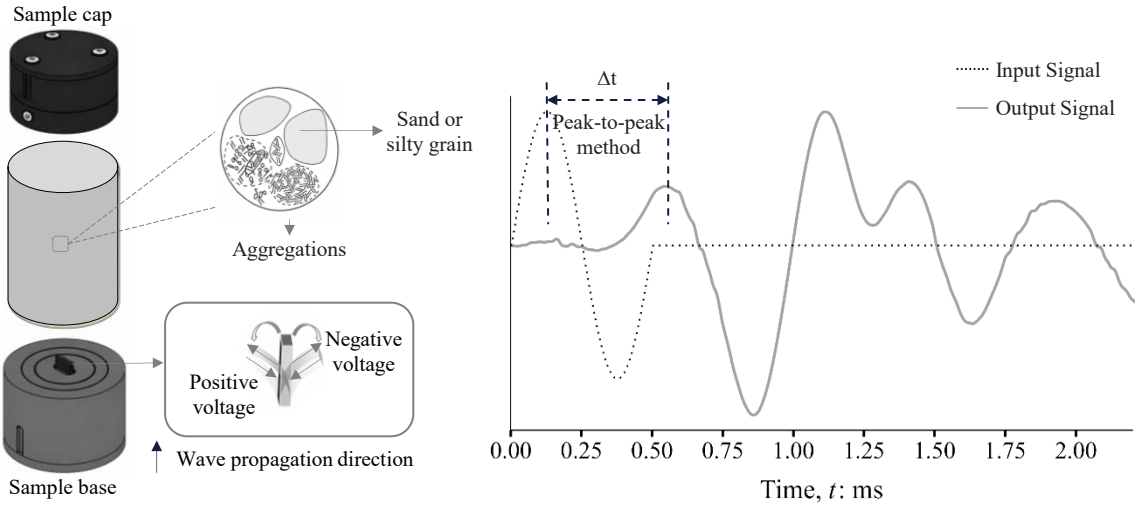

The shear wave velocity, V_s, was calculated as the ratio between the effective wave travel distance and the wave propagation time, according to the classical expression given in Equation 1-1. The effective propagation distance, L_{tt}, was defined as the tip-to-tip distance between the piezoelectric elements installed at the opposite ends of the specimen,

corresponding to the effective path travelled by the shear wave through the soil. This definition was maintained throughout the experimental program to ensure consistency in estimating shear wave velocity for the different hydraulic states investigated.

$$V_S = \frac{L_{tt}}{t} \qquad \text{Equation 1-1}$$

The determination of the wave propagation time, *t*, was carried out using the peak-to-peak criterion, based on the analysis of the recorded output signal. This procedure involved identifying the time interval between characteristic peaks of the input and output signals, as illustrated in Figure 1-3b. The application of the peak-to-peak criterion, together with its main advantages and limitations, is discussed in detail in the studies by Viana da Fonseca et al. (2009) and Ogino et al. (2015).

Based on the shear wave velocity, the small-strain shear modulus, G_0, was estimated using the classical relationship presented in Equation 1-2, which relates soil stiffness to total density and shear wave velocity. In this expression, *r* denotes the total density of the soil at the hydraulic state considered. Values of G_0 were determined at each stage of the drying and wetting cycles, allowing the assessment of stiffness variations associated with changes in the hydraulic state throughout the experimental programme.

$$G_{max} = \rho V_s^2 \qquad \text{Equation 1-2}$$

1.3. TEST RESULTS

1.3.1. Bender element response under different structural conditions

Accordingly, higher dry unit weight is accompanied by a reduced variation in the peak-to-peak travel time and by increased values of shear-wave velocity Vs and small-strain shear modulus G0, as shown in Figure 1-4 b and c.

Figure 1-4a presents the signals obtained from the bender element tests for the IUC, RUC, and CUC specimens, corresponding, respectively, to the undisturbed, remoulded, and compacted states. The responses associated with the IUC and RUC specimens are very similar, indicating comparable levels of small-strain stiffness under these two structural conditions. In contrast, the CUC specimen exhibits a markedly shorter shear-wave arrival time, reflecting a stiffer mechanical response. This response is associated with the lower void ratio achieved through compaction, which enhances interparticle contact (Ge et al., 2024; Kim et al., 2023). Accordingly, higher dry unit weight is accompanied by a reduced variation in the peak-to-peak travel time and by

increased values of shear-wave velocity Vs and small-strain shear modulus G0, as shown in Figure 1-4 b and c.

Figure 1-4. Initial conditions of the IUC, RUC, and CUC specimens: (a)BE signals, (b) Vs, and (c) G0.

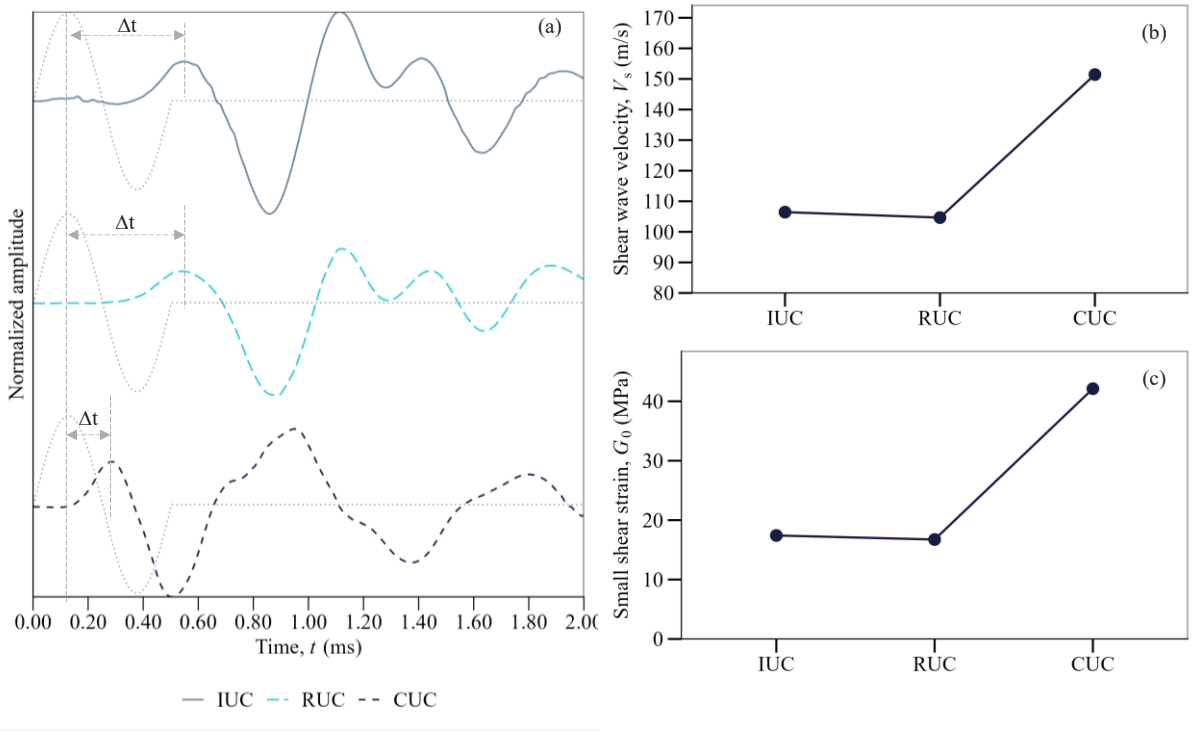

1.3.2. Structural response of the undisturbed soil at small strains during hydraulic cycling

Figure 1-5a presents the bender element signals obtained from the undisturbed specimen subjected to drying–wetting cycles. The experimental programme was initiated with the drying path, followed by wetting, allowing a direct assessment of the soil response along distinct hydraulic trajectories.

As shown in Figure 1-5b, drying resulted in a progressive reduction in void ratio. This process was accompanied by an increase in shear wave velocity, V_S (Figure 1-5c), and in the small-strain shear modulus, G_0 (Figure 1-5d). Accordingly, lower water contents are associated with higher values of V_S and G_0.

During the wetting path, an increase in void ratio is observed, together with a marked reduction in V_S and G_0. For a given water content, the values measured during wetting differ from those obtained along the drying path, highlighting the presence of hydraulic hysteresis in the mechanical response of the material.

Figure 1-5. Bender element results for the undisturbed specimen during drying–wetting cycles: (a) representative signals; (b) void ratio; (c) V_s; and (d) G_0, as functions of water content.

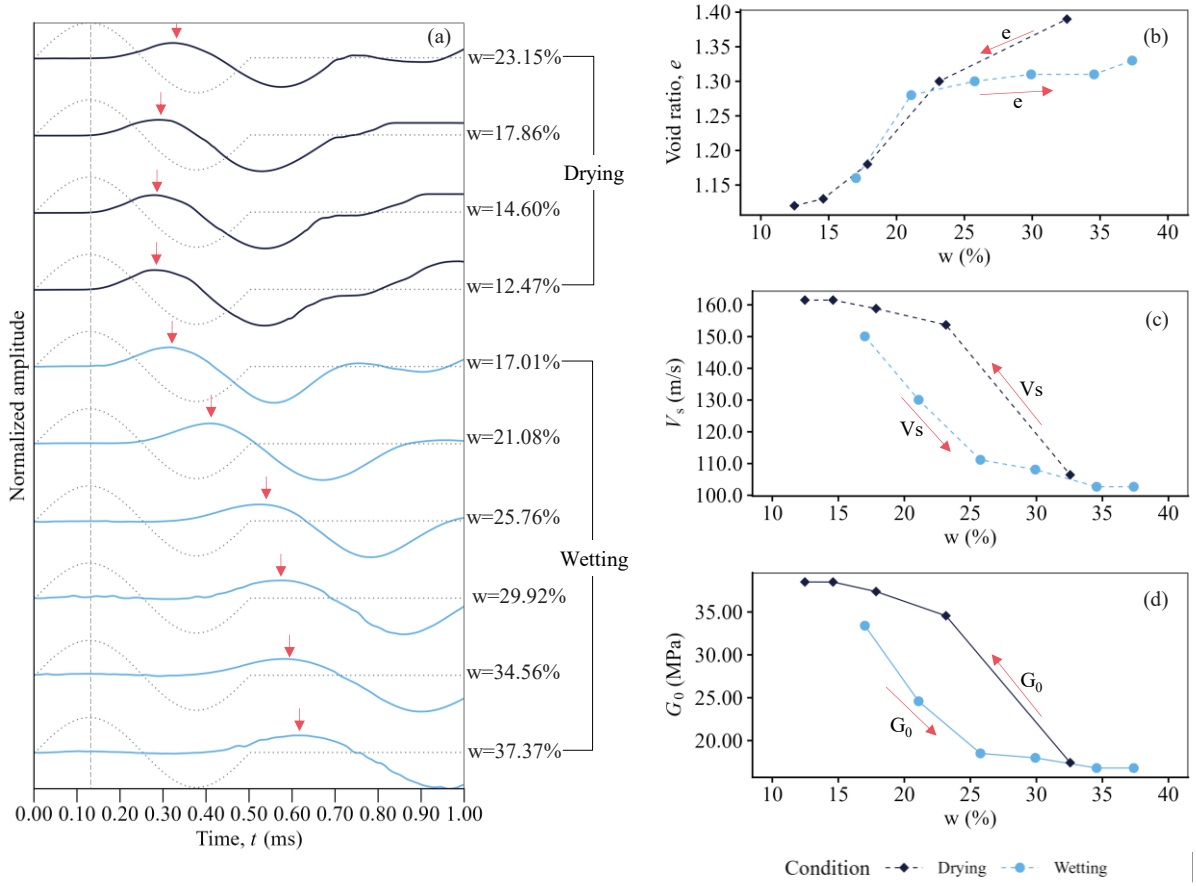

1.3.3. Small-strain structural response of the remoulded soil during hydraulic cycling

Figure 1-6a presents the bender element results obtained for the remoulded specimen. It is noted that the drying path could be completed; however, despite testing in triplicate, the specimen consistently disintegrated at the second measurement point along the wetting path.

Figure 1-6. Bender element results for the remoulded specimen during drying–wetting cycles: (a) representative signals; (b) void ratio; (c) V_s; and (d) G_0, as functions of water content.

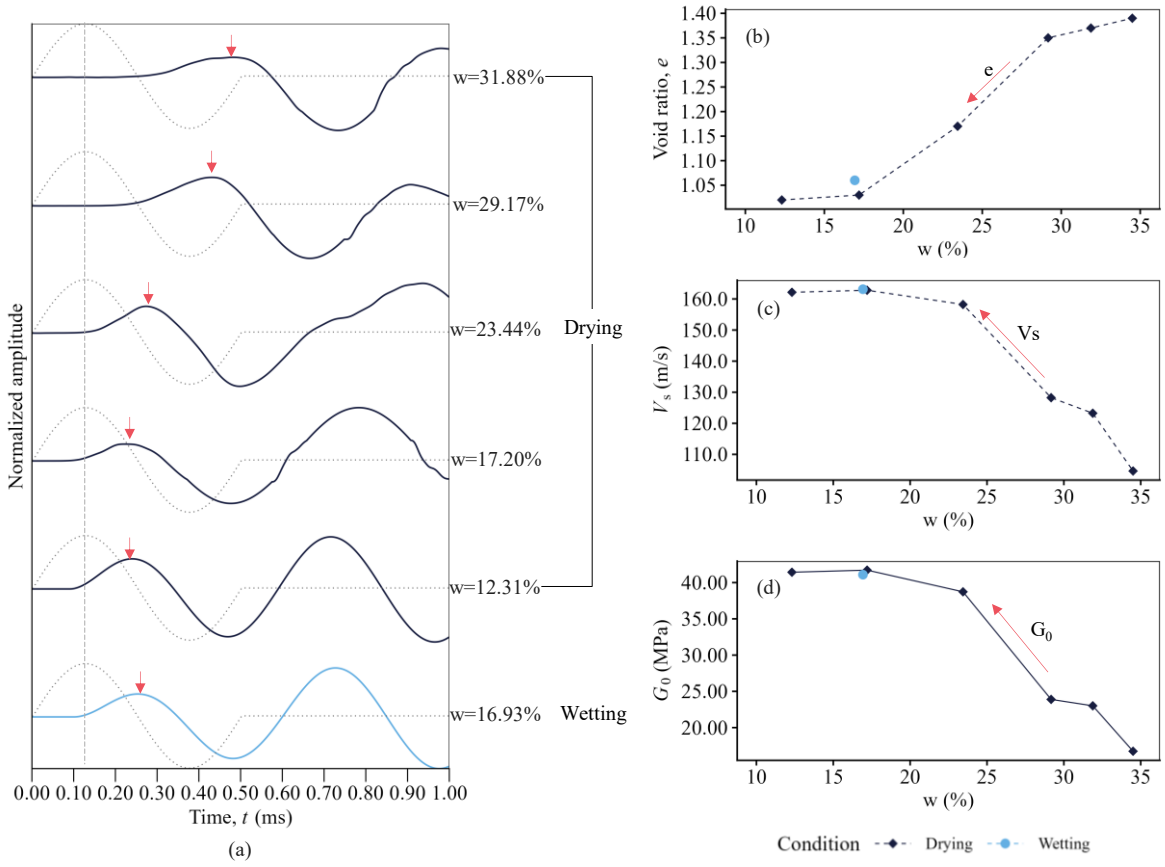

The remoulded specimen was prepared by air-drying the soil to its hygroscopic water content, followed by the addition of distilled water until reaching the water content of the undisturbed specimen. The material was then remoulded by pressing to achieve the same void ratio. Owing to the high void ratio of approximately e = 1.35, the remoulded specimen exhibited a porous structure that differed significantly from that of the undisturbed soil. The remoulding process resulted in the loss of the natural cementation inherent to the lateritic soil, rendering the material mechanically unstable and highly susceptible to structural breakdown upon wetting.

Along the drying path, a progressive reduction in void ratio was observed (Figure 1-6b), accompanied by an increase in shear wave velocity, V_s (Figure 1-6c), and, consequently, an increase in the small-strain shear modulus, G_0 (Figure 1-6d). These results indicate that, although the remoulded soil exhibits a stiffness gain during drying, its structural integrity under wetting conditions is markedly reduced when compared with the undisturbed specimen.

1.3.4. Small-strain structural response of the compacted soil during hydraulic cycling

The bender element results for the compacted specimen are presented in Figure 1-7a. In this case, the specimen was initially subjected to wetting, followed by a drying stage and a subsequent wetting path, allowing the evaluation of the material response along different hydraulic trajectories. As shown in Figure 1-7b, the largest variability in void ratio occurs at water contents above approximately 16%, within which the most pronounced volumetric expansion and contraction are observed. For water contents lower than 16%, variations in e are relatively limited. Consistent with the volumetric behaviour, the largest variations in shear wave velocity, V_s (Figure 1-7c), and in the small-strain shear modulus, G_0 (Figure 1-7d), also occur at water contents above 16%, whereas more stable values are observed at lower water contents.

Figure 1-7. Bender element results for the remoulded specimen during drying–wetting cycles: (a) representative signals; (b) void ratio; (c) V_s; and (d) G_0, as functions of water content.

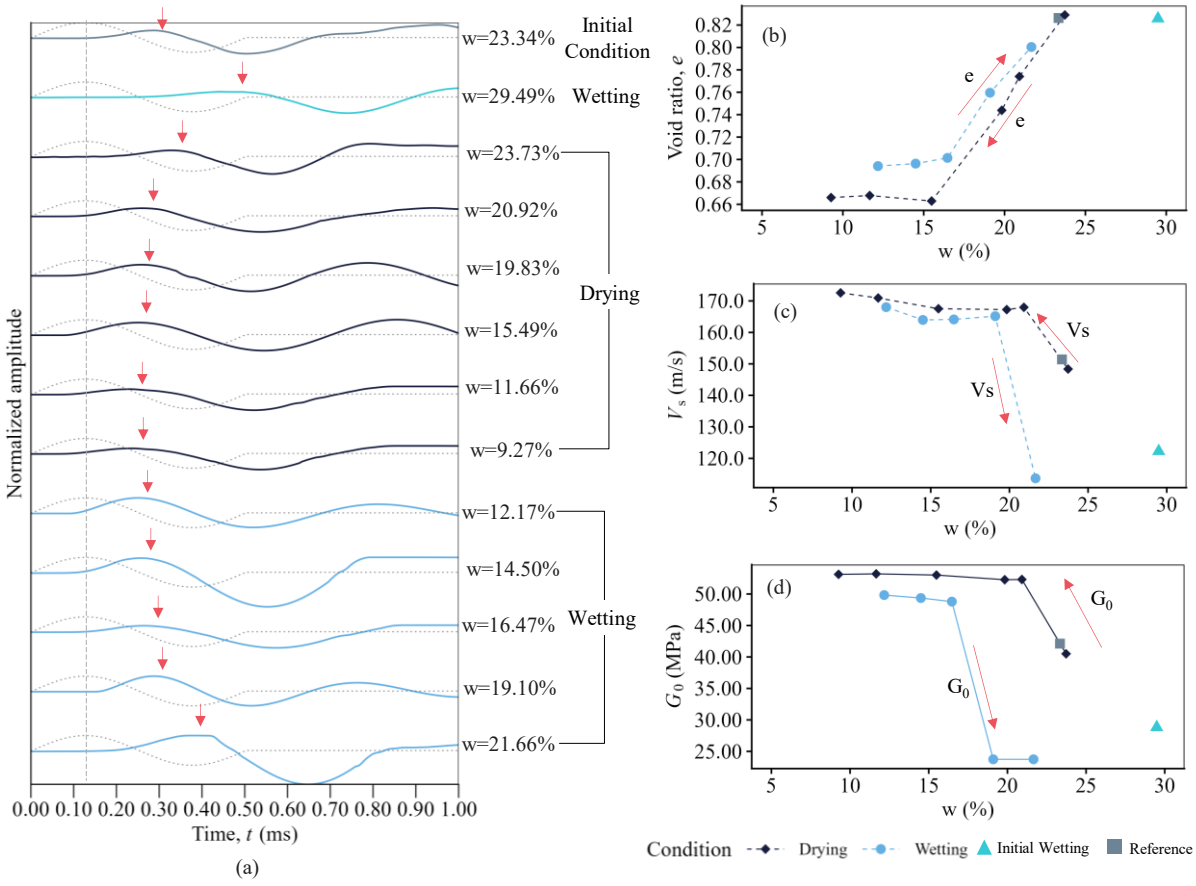

1.4. DISCUSSION

Figure 13 8c and d present the evolution of the small-strain shear modulus, G0, as a function of water content during drying and wetting, respectively. Overall, G0 increases with decreasing water content and decreases as water content increases. Regardless of the hydraulic path, the compacted specimen exhibits higher G0 values when compared with the remoulded and undisturbed specimens.

Along the drying path, two distinct stages can be identified. For the compacted specimen, G0 remains approximately constant at about 52.8 MPa for water contents up to 20%, whereas for higher water contents, a marked reduction is observed, decreasing to 40.5 MPa at 23.73%, corresponding to a reduction of approximately 23%. For the remoulded specimen, variations in G0 are limited for water contents up to 17%, with an average value of approximately 41.6 MPa.

As wetting progresses, G0 decreases progressively from 41.6 MPa at 17% to 38.73 MPa at 23.44%, 23.89 MPa at 29.17%, 23.01 MPa at 31.88%, and 16.74 MPa at 34.50%. For the undisturbed specimen, G0 remains relatively stable up to a water content of 17.86%, with an average value of approximately 38.1 MPa, followed by a reduction to 34.6 MPa at 23.15% and to 17.42 MPa at 32.56%. As observed, the variation of G_0 is not uniform along the drying and wetting paths.

Similar non-uniform behaviour has been reported in the literature when comparing the evolution of G_0 with matric suction, which also exhibits distinct responses along drying and wetting trajectories

Figure 1-8a shows the variation of void ratio along the drying path for the IUC, RUC and CUC specimens. The remoulded specimen exhibits a more pronounced variation in void ratio when compared with the undisturbed specimen; however, this behaviour becomes significant only at water contents above approximately 18%, whereas changes in e are limited below this threshold.

A similar trend is observed for the compacted specimen, for which variations in void ratio remain small within the water content range of 9–16%, becoming more pronounced at water contents exceeding 16%.

Figure 13 8c and d present the evolution of the small-strain shear modulus, G0, as a function of water content during drying and wetting, respectively. Overall, G0 increases with decreasing water content and decreases as water content increases. Regardless of the hydraulic path, the compacted specimen exhibits higher G0 values when compared with the remoulded and undisturbed specimens.

Along the drying path, two distinct stages can be identified. For the compacted specimen, G0 remains approximately constant at about 52.8 MPa for water contents up to 20%, whereas for higher water contents, a marked reduction is observed, decreasing to 40.5 MPa at 23.73%, corresponding to a reduction of approximately 23%. For the remoulded specimen, variations in G0 are limited for water contents up to 17%, with an average value of approximately 41.6 MPa.

As wetting progresses, G0 decreases progressively from 41.6 MPa at 17% to 38.73 MPa at 23.44%, 23.89 MPa at 29.17%, 23.01 MPa at 31.88%, and 16.74 MPa at 34.50%. For the undisturbed specimen, G0 remains relatively stable up to a water content of 17.86%, with an average value of approximately 38.1 MPa, followed by a reduction to 34.6 MPa at 23.15% and to 17.42 MPa at 32.56%. As observed, the variation of G_0 is not uniform along the drying and wetting paths.

Similar non-uniform behaviour has been reported in the literature when comparing the evolution of G_0 with matric suction, which also exhibits distinct responses along drying and wetting trajectories

Figure 1-8. e and G_0 as functions of water content for IUC, RUC, and CUC: (a) e–drying; (b) e–wetting; (c) G_0–drying; and (d) G_0–wetting.

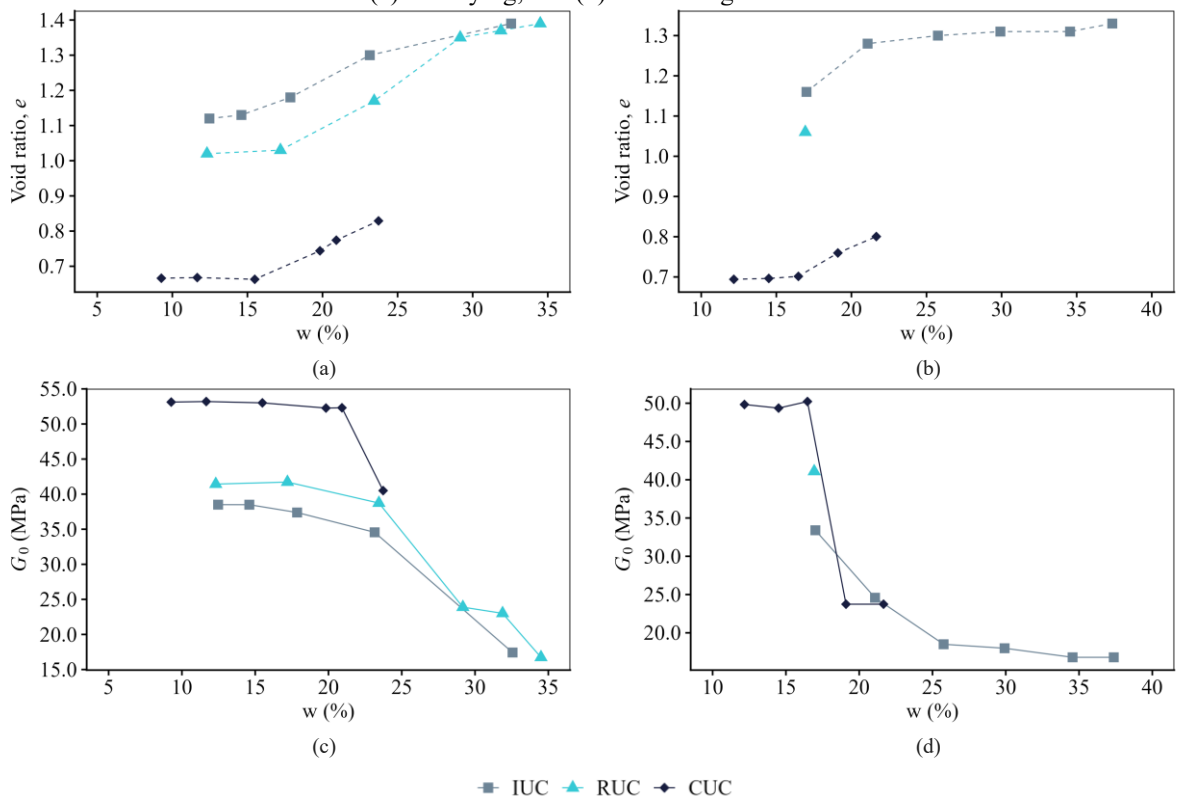

1.5. CONCLUSIONS

The results confirm that small-strain shear stiffness is governed by hydraulic state under unconfined conditions, exhibiting a systematic increase during drying and a reduction during wetting. This behaviour highlights the transient nature of initial stiffness in tropical unsaturated soils, where variations in matric suction directly modify the ability of the granular skeleton to transmit shear waves and to resist very small deformations.

The mechanical response exhibits hydraulic hysteresis, indicating that stiffness cannot be represented as a single-valued function of water content. For a given water content, stiffness values obtained after drying differ from those measured after wetting, particularly in the undisturbed condition. This observation implies hydraulic memory and dependence on the redistribution history of water within pores and aggregates. Consequently, interpretations and constitutive approaches based solely on moisture content may overlook relevant information when drying–wetting cycles are involved.

Compaction at standard compaction energy produces consistently higher stiffness compared with the other structural conditions, reflecting reduced void ratio and improved interparticle contact efficiency. Furthermore, stiffness sensitivity to water content is non-linear. The compacted condition shows limited variation at low water contents, followed by pronounced degradation beyond a threshold range, with the most significant reductions occurring at water contents above approximately sixteen percent. This pattern suggests that changes in hydraulic regime, rather than gradual moisture variation alone, control stiffness degradation within specific ranges.

The remoulded condition exhibited structural instability during wetting, with recurrent disaggregation despite repeated testing, associated with the loss of natural cementation and elevated porosity. This indicates that reconstitution, even when reproducing the field void ratio, does not preserve the bonding mechanisms and internal organisation responsible for the stability of the undisturbed material, leading to substantially different initial stiffness and wetting-induced evolution.

Overall, the results demonstrate that microstructural condition simultaneously governs the magnitude of initial stiffness and its dependency on hydraulic path. Structural state should therefore be treated as a first-order variable in stiffness-based assessments of lateritic soils subjected to hydroclimatic variability. The experimental evidence supports the conclusion that design and interpretation frameworks neglecting drying–wetting history may underestimate relevant field stiffness variations, particularly in aggregated and naturally cemented tropical soils

REFERENCES

ASTM D2487-17. Standard Practice for Classification of Soils for Engineering Purposes (Unified Soil Classification System). 2020.

Booshehrian A, Wan R, Su X. Hydraulic variations in permafrost due to open-pit mining and climate change: a case study in the Canadian Arctic. Acta Geotech 2020;15:883–905. https://doi.org/10.1007/s11440-019-00786-x.

Camacho-Tauta J, Santos JA, da Fonseca AV. Two Bender Receivers Frequency Domain Analysis in Resonant Column Tests, American Society of Civil Engineers (ASCE); 2014, p. 72–82. https://doi.org/10.1061/9780784413425.009.

Camacho-Tauta JF, Cascante G, Da Fonseca AV, Santos JA. Time and frequency domain evaluation of bender element systems. Geotechnique 2015;65:548–62. https://doi.org/10.1680/geot.13.P.206.

Dong Y, Lu N, McCartney JS. Unified Model for Small-Strain Shear Modulus of Variably Saturated Soil. Journal of Geotechnical and Geoenvironmental Engineering 2016;142. https://doi.org/10.1061/(ASCE)GT.1943-5606.0001506.

Gao Z, Kong L, Yan J, Wang S. Effects of drying–wetting cycles on small-strain stiffness characteristics of fissured clay. Journal of Rock Mechanics and Geotechnical Engineering 2025;17:4618–31. https://doi.org/10.1016/j.jrmge.2024.09.023.

Ge M, Han X, Yang R, Zhu C. Small-strain stiffness of compacted loess upon wetting, drying and loading: Experiments and model interpretation. Transportation Geotechnics 2024;48:101341. https://doi.org/10.1016/j.trgeo.2024.101341.

Gu X, Yang J, Huang M. Laboratory measurements of small strain properties of dry sands by bender element. Soils and Foundations 2013;53:735–45. https://doi.org/10.1016/j.sandf.2013.08.011.

Hoyos LR, Suescún-Florez EA, Puppala AJ. Stiffness of intermediate unsaturated soil from simultaneous suction-controlled resonant column and bender element testing. Eng Geol 2015;188:10–28. https://doi.org/10.1016/j.enggeo.2015.01.014.

Insana A, Uzielli M, Bračko T, Pourfatollah A, Vitale P, Žlender B, et al. A framework for climate-adaptive geotechnical analysis and design. Bulletin of Engineering Geology and the Environment 2025;84:590. https://doi.org/10.1007/s10064-025-04628-x.

Kandalai S, John NJ, Patel A. Effects of Climate Change on Geotechnical Infrastructures — state of the art. Environmental Science and Pollution Research 2023;30:16878–904. https://doi.org/10.1007/s11356-022-24788-7.

Kilsby C, Glendinning S, Hughes PN, Parkin G, Bransby MF. Climate-change impacts on long-term performance of slopes. Proceedings of the Institution of Civil Engineers - Engineering Sustainability 2009;162:59–66. https://doi.org/10.1680/ensu.2009.162.2.59.

Kim M, Lee C, Kim J-U, Choo H. Use of shear wave velocity for assessing engineering properties of compacted bentonite after swelling. Sci Rep 2023;13:15705. https://doi.org/10.1038/s41598-023-42779-7.

Lee J-S, Santamarina JC. Bender Elements: Performance and Signal Interpretation 2005. https://doi.org/10.1061/ASCE1090-02412005131:91063.

Liu X, Zou D, Liu J, Zhou C, Zheng B. Experimental study to evaluate the effect of particle size on the small strain shear modulus of coarse-grained soils. Measurement 2020;163:107954. https://doi.org/10.1016/j.measurement.2020.107954.

Masutti G, Falcão P, Baroni M, Barbosa R, Souza T. Load capacity evaluation of different typologies of short and small diameter piles. Soils and Rocks 2023;46:e2023004722. https://doi.org/10.28927/SR.2023.004722.

Ng CWW, Yung SY. Determination of the anisotropic shear stiffness of an unsaturated decomposed soil. Géotechnique 2008;58:23–35. https://doi.org/10.1680/geot.2008.58.1.23.

Ngoc TP, Fatahi B, Khabbaz H. Impacts of Drying-Wetting and Loading-Unloading Cycles on Small Strain Shear Modulus of Unsaturated Soils. International Journal of Geomechanics 2019;19. https://doi.org/10.1061/(ASCE)GM.1943-5622.0001463.

NOGAMI JS, VILLIBOR DF. Uma nova classificação de solos para finalidades rodoviárias. Anais Simpósio Brasileiro de solos tropicais em engenharia, Rio de Janeiro: 1981.

Ogino T, Kawaguchi T, Yamashita S, Kawajiri S. Measurement deviations for shear wave velocity of bender element test using time domain, cross-correlation, and frequency domain approaches. Soils and Foundations 2015;55:329–42. https://doi.org/10.1016/j.sandf.2015.02.009.

Olaiz A, Mosawi M, Zapata C. An improved framework for volume change of shrink/swell soils subjected to time-varying climatic effects. Soils and Rocks 2021;44:1–14. https://doi.org/10.28927/SR.2021.065621.

Pascoal P, Sagrilo A, Baroni M, Specht L, Pereira D. Lateritic soil deformability regarding the variation of compaction energy in the construction of pavement subgrade. Soils and Rocks 2023;46:e2023009922. https://doi.org/10.28927/sr.2023.009922.

Pascoal PT, Sagrilo AV, Baroni M, Specht LP, Pereira D da S. Evaluation of the influence of compaction energy on the resilient behavior of lateritic soil in the field and laboratory. Soils and Rocks 2021;44. https://doi.org/10.28927/SR.2021.071321.

Pham TA. Climate change impacts on geotechnical infrastructure: role of unsaturated soil mechanics for adaptation. Front Built Environ 2025;11. https://doi.org/10.3389/fbuil.2025.1666334.

Pham TA, Sutman M. Modeling the combined effect of initial density and temperature on the soil–water characteristic curve of unsaturated soils. Acta Geotech 2023;18:6427–55. https://doi.org/10.1007/s11440-023-01920-6.

Shahgholian R, Viana da Fonseca A, Ferreira C. A simple approach for assessing the quality of bender elements. Géotechnique Letters 2025;15:283–8. https://doi.org/10.1680/jgele.24.00098.

Tetteh FK, Abbey SJ, Booth CA, Nukah PD. Current understanding and uncertainties associated with climate change and the impact on slope stability: A systematic literature review. Natural Hazards Research 2025;5:563–95. https://doi.org/10.1016/j.nhres.2025.01.011.

Viana da Fonseca A, Ferreira C, Fahey M. A framework interpreting bender element tests, combining time-domain and frequency-domain methods. Geotechnical Testing Journal 2009;32:91–107. https://doi.org/10.1520/gtj100974.

Viggiani G, Atkinson JH. Interpretation of bender element tests. Géotechnique 1995;45:149–54. https://doi.org/10.1680/geot.1995.45.1.149.

Villibor DF, Nogami JS. Pavimentos Econômicos: tecnologia do uso dos solos finos lateríticos. Editora Arte & Ciência; 2009.

Walker C, Heitor A, Clarke BG. Impact of drying-wetting cycles on the small strain behaviour of compacted clay. Transportation Geotechnics 2023;42:101063. https://doi.org/10.1016/j.trgeo.2023.101063.